



Original Paper

Detecting Land Subsidence Due to Groundwater Withdrawal in Aliabad Plain, Iran, Using ESA Sentinel-1 Satellite Data

Ali Edalat,¹ Mahdi Khodaparast ^{1,3} and Ali M. Rajabi²

Received 12 January 2019; accepted 17 August 2019
Published online: 27 August 2019

In the present study, ground subsidence in the Aliabad plain (central Iran) was investigated using differential synthetic aperture radar interferometry. The data used for this purpose were Sentinel 1 images acquired during the time range from 24/03/2015 to 8/09/2016. Four interferogram pairs with high coherence were selected to minimize temporal decorrelation. The final analysis was performed in an area where there is sufficient hydrological and geological information. The results revealed that subsidence is a continuous phenomenon in the study area. The vertical displacement rate during the investigated period was estimated to be 178 mm/year. It was also noticed that the subsidence rate in the western part of the plain was higher than in other parts. Moreover, the effects of groundwater level decline, alluvium thickness, and transmissivity on the subsidence level were investigated. Overall, this research provides a correlation between the amount and distribution of land subsidence and effective factors for accurate detection of this phenomenon.

KEY WORDS: DInSAR, Sentinel 1, Subsidence, Aliabad plain, Qom.

INTRODUCTION

Land subsidence is referred to as downward deformation or settlement which could be of small displacement vector (Bates and Jackson 1987). In recent years, man-made activities such as loading induced by engineered structures, mining, and over-exploitation of underground fluids have majorly triggered land subsidence all around the world (Zhu et al. 2015). Today, the ever-increasing land subsidence caused by excessive groundwater pumping is considered as a global concern (Gambolati et al. 2006; Galloway and Burbey 2011). In Iran, most of the plains are in critical conditions due to the rapid

development of agriculture induced by rapid population growth, increasing water demand, water over-exploitation, and groundwater level decline. Land subsidence in Iran due to groundwater withdrawal is a critical issue in cities such as Tehran, Mashhad, Kashmar, Varamin, Kashan, Rafsanjan (Sharifikia 2010). Hence, ground deformation monitoring and investigating the mechanism of land subsidence for some of aquifers and plains in Iran are inevitable.

Qom, as a province located in the center of Iran, is located in the south of Tehran province, north of Isfahan province, east of the Markazi province, and west of Semnan province. Low rainfall, hot and dry climates, and geological conditions have made groundwater as the main source of water supply in this province (Rezaei Kalantari et al. 2013). The Aliabad plain, located in the boundary of the Qom and Markazi provinces, is a part of the Saveh County. This plain is fed by the Qarah-Chay river in the past. During 1996–2017, construction and

¹Department of Civil Engineering, University of Qom, Qom, Iran.

²Department of Engineering Geology, University of Tehran, Tehran, Iran.

³To whom correspondence should be addressed; e-mail: khodaparast@qom.ac.ir

increased storage of upstream dams and successive droughts have caused an increase in the number of agricultural wells and land subsidence due to groundwater withdrawal.

Non-similar changes in topographic elevation and slope of rivers, streams, and water transfer structures, the disruption of water resources consumption, and destruction of mainlines and structures are among the major effects of land subsidence (Holzer and Galloway 2005). In this regard, issues such as the detection of temporal progress, spatial distribution, and subsidence level are of critical importance (Bonì et al. 2015). There is an ever-growing increase in the use of remote sensing (RS) techniques in studying various phenomena. For example, differential synthetic aperture radar interferometry (DInSAR) is an advanced RS tool that is capable of mapping displacement changes in wide areas with lower cost compared to other common techniques such as repeat optical leveling and global positioning system (GPS) (Toms et al. 2014).

The introduction of the DInSAR technique and the launch of new satellites have found a special place among researchers. Bonì et al. (2015) studied severe land subsidence progress for a long period in southeast Spain using SAR images and advanced DInSAR techniques. They showed that subsidence is the consequence of groundwater level decline that has started several decades ago due to the over-exploitation of the aquifer in this area. In another study, Siles et al. (2015) investigated land deformation in the north of the Valley of Mexico using InSAR time series analysis with Envisat SAR images. They showed that the maximum subsidence rate in the region is 285 mm/year. Davoodijam et al. (2015) detected land subsidence in the Mahyar plain, Central Iran, through analysis of Envisat InSAR time series, and they showed a maximum subsidence rate of 9 cm/year during the study period. In a study by Ahmad et al. (2017) using Sentinel-1 SAR images, it was found that the main cause of land subsidence in the Quetta valley, Pakistan, is groundwater over-exploitation. The results obtained by that study revealed that the Quetta valley has experienced 10 to 20 mm subsidence during 2 years. Fiaschi et al. (2017) monitored land subsidence for a 25-year period in the Municipality of Ravenna (Italy) using DInSAR technique and reported the great potential of Sentinel-1A in conventional monitoring of land subsidence even on a local scale. In Iran, the destructive effects of land subsidence have also been reported in Tehran (Mahmoudpour et al. 2016),

Arak (Rajabi and Ghorbani 2016), Mahyar, Naysabour and Kashmar (Lashkaripour et al. 2010).

Despite the significance of land subsidence in Qom province, a limited number of studies have been conducted on this issue. Rajabi (2018) evaluated numerically land subsidence in some parts of the Aliabad plain during the period 2001–2013 and demonstrated that the plain has experienced a 0–76 cm subsidence during 12 years. In this study, using the geotechnical data acquired from the literature and engineering judgements, subsidence of an area of the Ali-Abad plain is numerically studied by PLAXIS Software.

In the present study, the subsidence in the Aliabad plain (center of Iran) is investigated using the DInSAR technique. The SAR images used for this purpose were acquired from Sentinel 1 satellites between 24/03/2015 and 8/09/2016. Geological and groundwater level change data for the period 2002–2015 were collected, analyzed, and compared with the land deformation information obtained from the satellite imagery. In this way, it is possible to better compare and understand spatial and temporal mechanisms governing the subsidence due to over-exploitation of the Aliabad aquifer system.

STUDY AREA

The Namak Lake basin, covering an area of 92,884 km², is located in the northwest of central Iran. This basin includes Tehran province and parts of Zanjan, Qom, Hamedan, Markazi, Qazvin, and Isfahan provinces. The establishment of Tehran megacity as the politico-economic center of Iran (in the north of study area) and its access to other areas has resulted in construction of major roads in this basin. Although this region contains only about 6.5% of Iran's area, 30% of the population of the nation lives there. The politico-economic place of this area and the presence of a large number of industrial, service, and cultural units in it have led to over-exploitation of available water resources. The Saveh basin, located between Qom and Markazi provinces, is one of the 41 Namak Lake basins. This basin is located almost in the center of these basins. Figure 1 shows the positions of the Namak Lake basin and the Saveh basin.

The Aliabad plain is part of the Saveh basin. The areas of plain and aquifer in Aliabad are 1712 and 1344 km², respectively. Because the generated interferograms cover only a part of the Saveh basin,

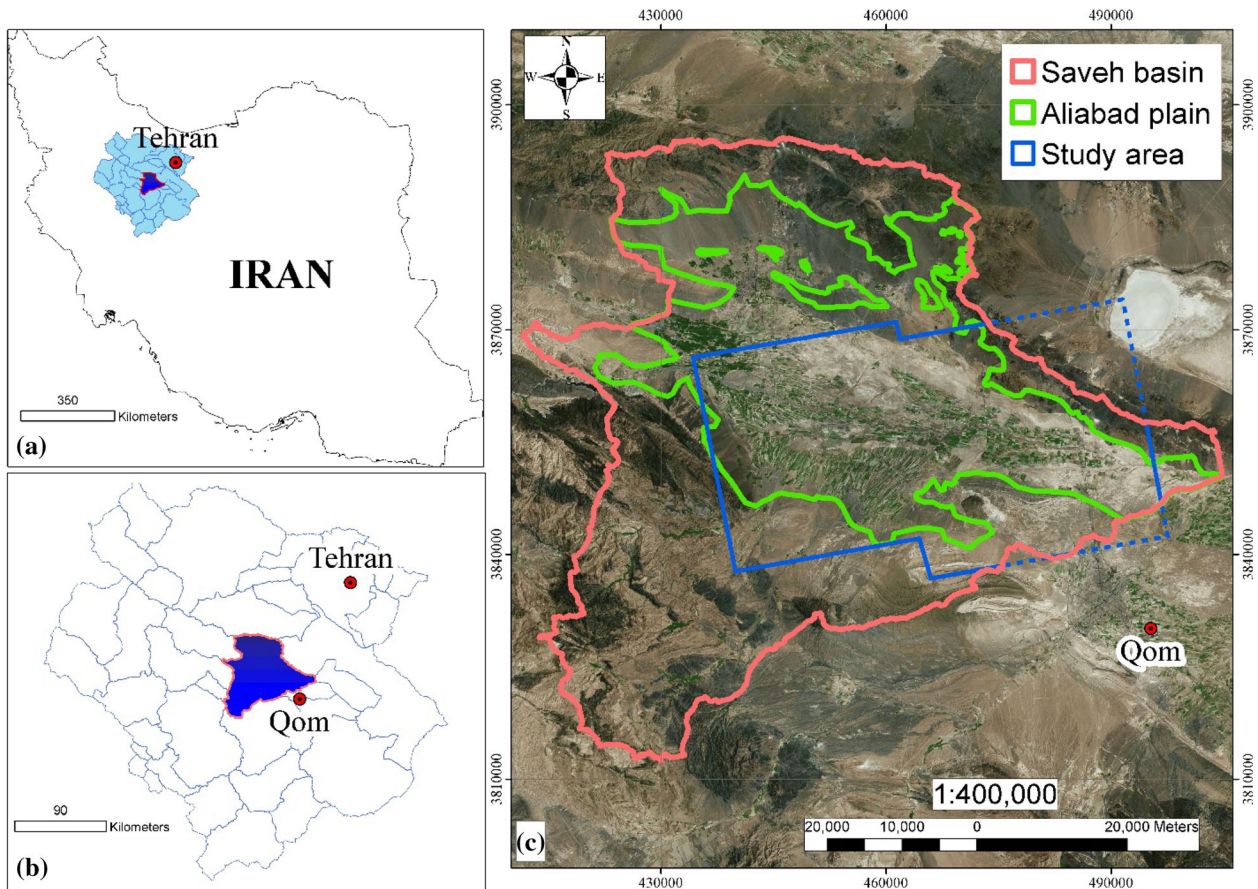


Figure 1. (a) Position of the Namak Lake basin in Iran. (b) Position of the Saveh basin in the Namak Lake basin. (c) Position of the Aliabad plain and study area in the Saveh basin.

the study area was chosen for having complete coverage of the interferogram images as well as sufficient hydrological and geological information (Fig. 1c).

The geological setting of the Saveh basin is presented in Figure 2. In the western part of this basin, where rivers flow through the Aliabad plain, alluvial deposits have accumulated due to significant river flow and to reduction in slope gradient. From the west to the east, alluvial sediment texture turns out to be fine-grained silt and clay. The plain is mostly covered by agricultural lands previously fed by the Qarah-Chay River. Following the construction of the Saveh dam in 1994, the Qarah-Chay River was dry most of the year and became a seasonal river, resulting in the excessive use of groundwater in the plain. The hydrograph of Ali-

abad plain for 1990 to 2015 period is shown in Figure 3 (Water Resources Report of Saveh Study Area 2013). During the 25-year period, the groundwater level in this plain has declined 34.13 m with an average annual decline of 1.35 m. This water level drop has led to subsidence in the Aliabad plain, which is accompanied by features such as an opening in the margin of the plain, disturbances of lifelines (i.e., roads, railway, and pipelines), and wall cracking (Fig. 4).

DATA AND METHOD

This section explains how the satellite data used are converted to ground surface displacement and directly geocoded into a map projection. For this

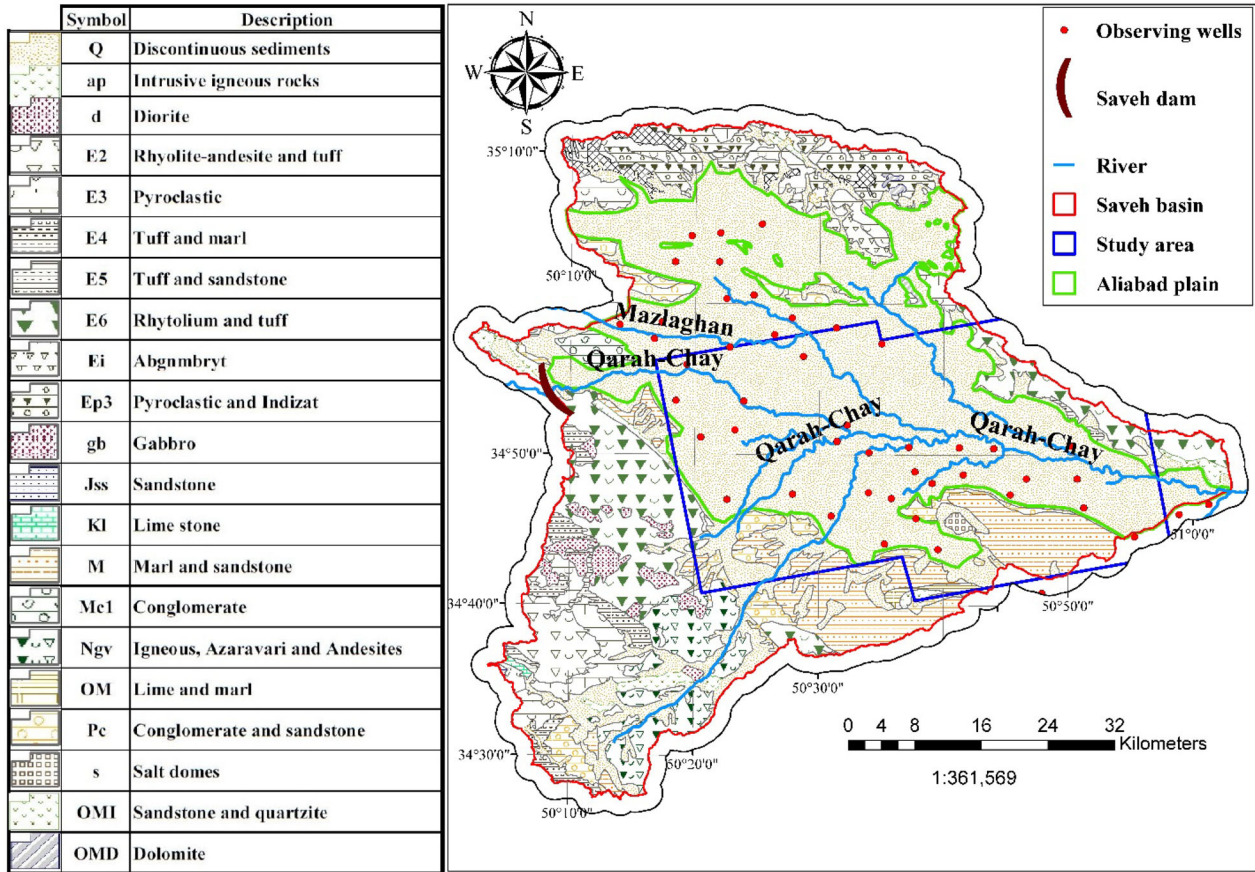


Figure 2. Geological setting of the Saveh basin (Water Resources Report of Saveh Study Area 2013).

purpose, the needed characteristics and data were acquired from the Sentinel-1 satellite and the process employed to convert them to ground’s surface displacement was described. In the study area, GPS stations have not been established. In addition, available leveling data are not sufficiently accurate to be used safely.

Sentinel-1 Interferometric Wide Products

Sentinel-1 is a space mission developed by the European Space Agency (ESA) in the framework of the Copernican Program. The mission includes two satellites. Sentinel-1A was launched on 3 April 2014, and Sentinel-1B was launched in early 2016 (Sentinel-1 2016). Sentinel-1A, depending on the desired target and application, captures SAR images in four different modes. Interferometric wide (IW) swath

mode is the default acquisition mode over land that obtains data with a 250 km swath and a 5 m × 20 m resolution. IW mode creates three sub-swaths with ~ 2 km overlap using novel terrain observation by progressive scans SAR mode. Each sub-swath image subtends a series of separate single look complex (SLC) image called bursts (Fig. 5; De Zan and Guarnieri 2006).

Satellite Images

We used 17 Sentinel-1A IW SLC SAR images acquired in ascending passes from 24 March 2015 to 9 August 2016. The level-1 images were downloaded from the Sentinel-1 Scientific Data Hub (Sentinel-1 Scientific Data Hub 2016). Each of the downloaded IW SLC images consists of three sub-swaths (i.e., IW1, IW2, and IW3). Each sub-swath is also divided

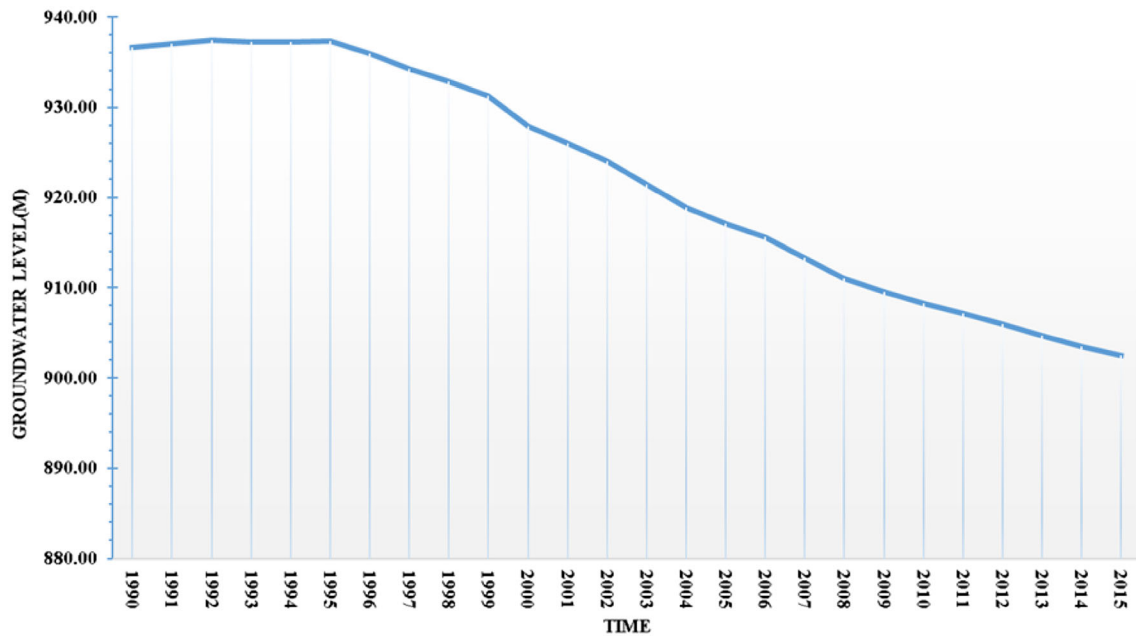


Figure 3. Hydrograph of Aliabad plain for the period 1990–2015 (Water Resources Report of Saveh Study Area 2013).

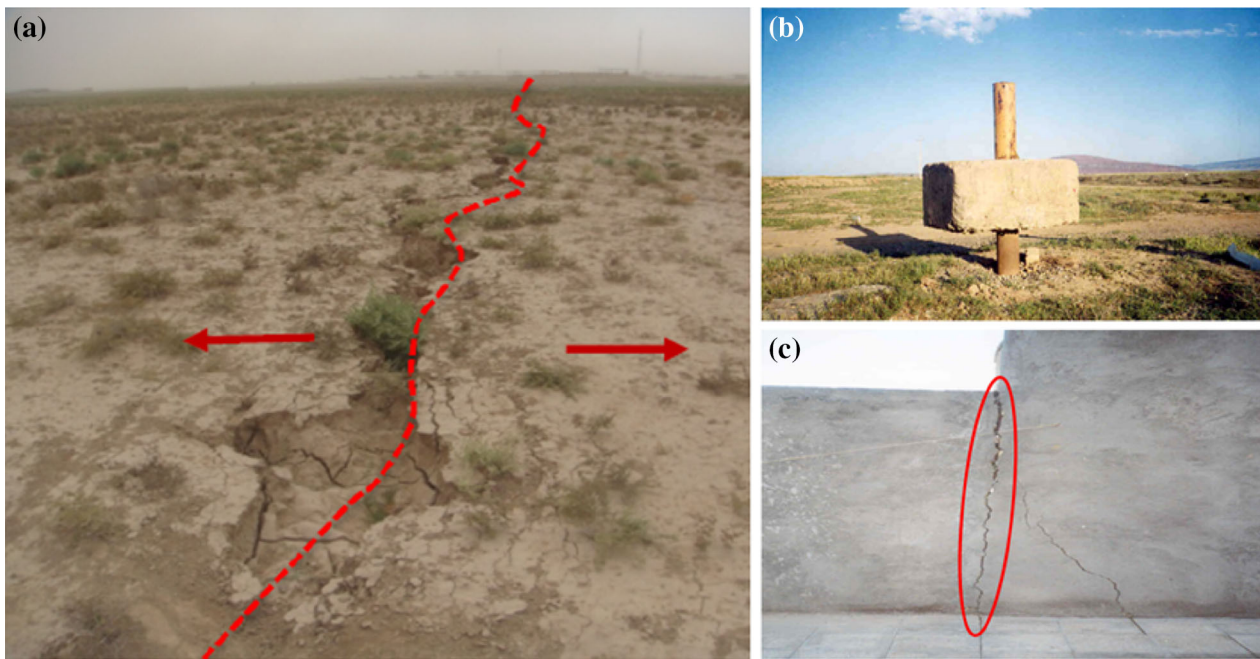


Figure 4. The consequences of subsidence phenomenon in the Aliabad plain: (a) opening in the margin of the Aliabad plain; (b) subsidence in the vicinity of piezometers; and c wall cracks.

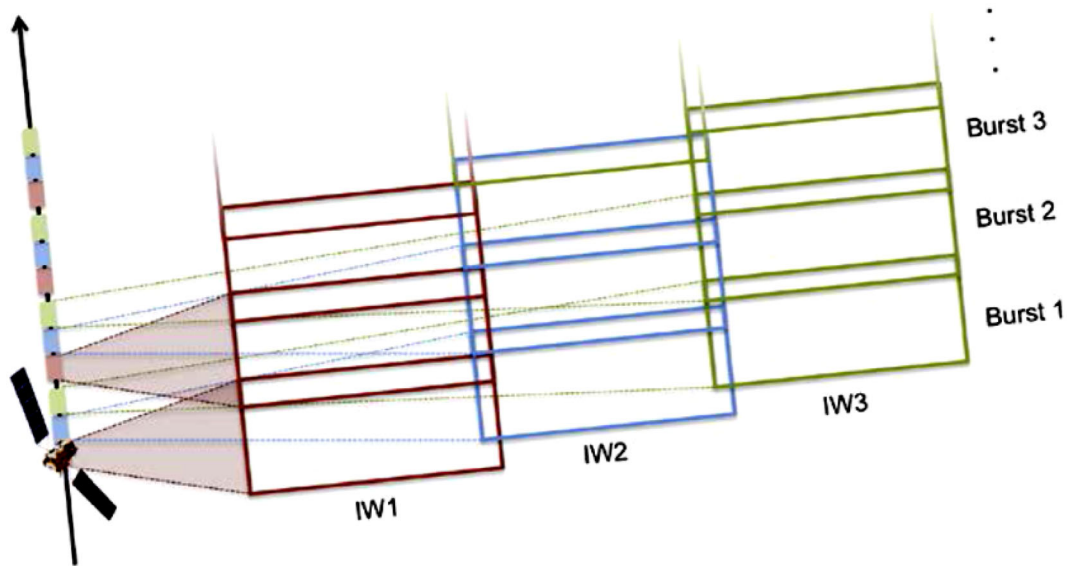


Figure 5. Sentinel-1 burst structure with small overlaps between bursts and sub-swaths (Wegmüller et al. 2016).

into nine bursts, and each burst is processed as a separate SLC image (Fig. 6). Because the study area is located in more than one burst, it was necessary to merge the bursts and create a wide-area IW product that covers the study area. This process, which is called co-registration, is required when multiple images cover the same region and a time series of pixel values needs to be analyzed. For this purpose, because it is not important which image is taken as the reference, the first image (by date) was used as the 161 reference and the others were co-registered to it.

Figure 7 presents the normal and temporal baselines of the Sentinel-1A IW SLC SAR images used in this study compared to the first image. In this graph, the pairs corresponding to the threshold are denoted by the straight lines. All pairs formed had the maximum normal and temporal baselines of 45% and 90 days, respectively. This threshold allows maximization of spatial coherence and the phase contribution due to Digital Elevation Map (DEM) errors (Yan et al. 2012). Furthermore, in this study, ASTER Global DEM with spatial resolution of 20 m was used.

Interferogram Analysis

DInSAR is a practical approach to monitor land deformations. Accordingly, the persistent scat-

ter interferometry (PS-InSAR) is the enhanced form of the DInSAR by which atmospheric effects are filtered. However, the PS-InSAR technique can be implemented in regions where the PS object can be identified similar to urban areas. Consequently, as the Ali-Abad plain lacks good persistence scatters, the DInSAR technique has been applied in this study.

Moreover, concerning atmospheric effects, it should be mentioned that the central parts of Iran are characterized by low of water vapor and there are almost no clouds. Anyhow, the atmospheric conditions (water vapor and cloud) have been taken into account prior to registering the Sentinel-1 data.

An interferogram is an image that shows the phase difference between two SAR images of the same area at different times taken from the same position. The observed phase (ϕ_{int}) is the sum of several contributions:

$$\phi_{int} = \phi_{Topography} + \phi_{Change} + \phi_{Movement} + \phi_{Atmosphere} + \phi_{Noise}$$

The objective of differential interferometry (DInSAR) is to extract the displacement one ($\phi_{Movement}$) from different components. In this study, passes 1 (master image) and 2 (slave image) in combination with a DEM (for subtracting the topography induced fringes) were considered to generate differential interferograms.

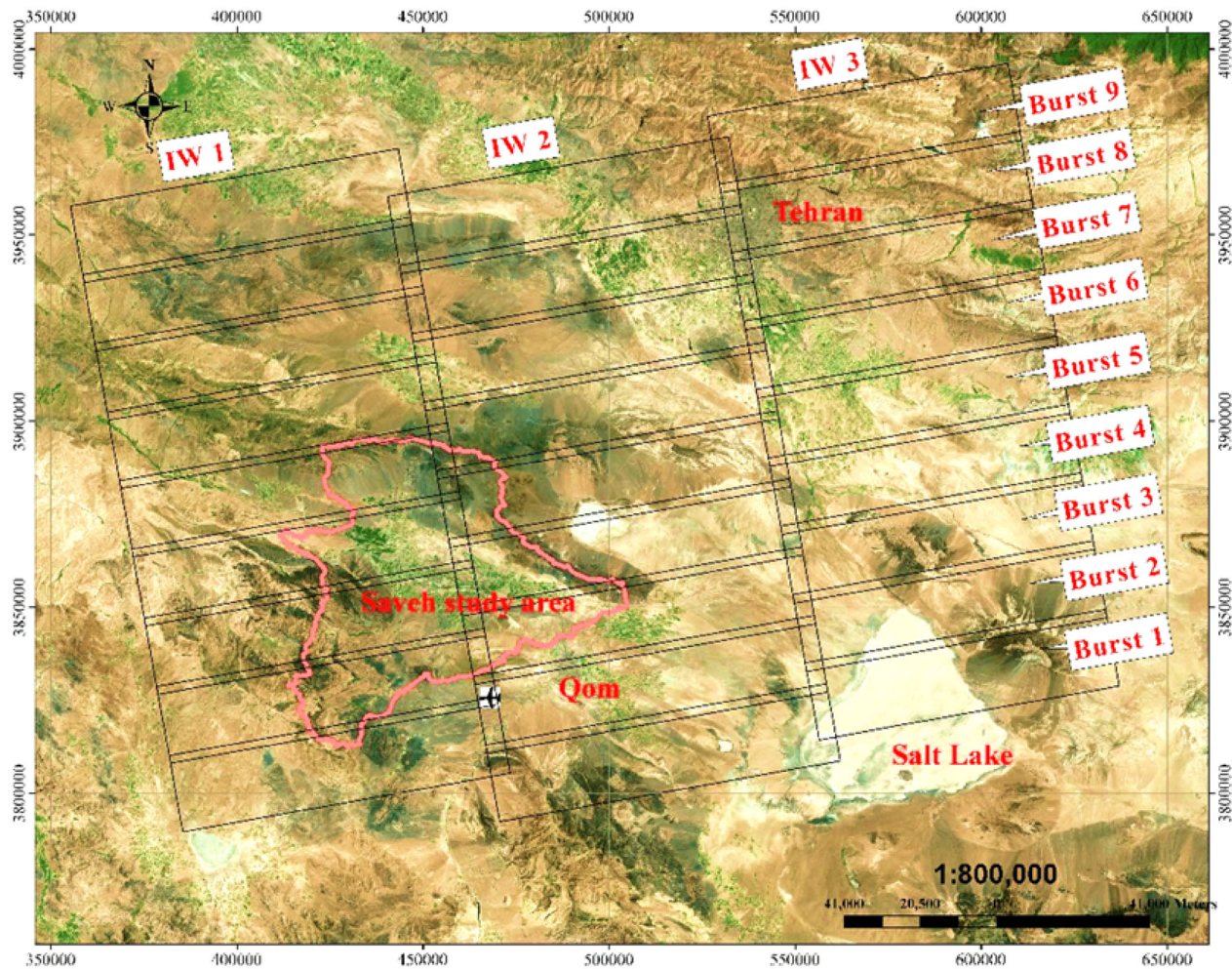


Figure 6. Sentinel-1 SLC image showing sub-swath IW1, IW2, and IW3, and position of study area.

The software ENVI SAR scape 5.2 (Sarmap 2015) was used for processing of IW-SLC images of the study area. A long-time baseline and the presence of vegetation have resulted low coherence in some parts of the study area. In order to minimize the temporal decorrelation effects and to generate strongly coherent interferograms for DInSAR processing chain, we selected four interferogram pairs (t_1 to t_4) with strong coherence. In addition, to study the effect of underground water change and thickness of alluvium on the subsidence level, the first and last images were used (t_5). Normal and temporal baselines and average coherence per interferogram of the study area are presented in Table 1. The range of image coherence values is between 0 and 1,

denoting areas with the lowest and the highest coherence, respectively. The estimated coherence is a function of systematic spatial decorrelation (i.e., additive noise) and temporal decorrelation between master and slave acquisitions.

In the next step, the reference DEM was given as input for removing topography from an interferogram. The ASTER DEM was used to produce differential interferograms containing subsidence fringes. Furthermore, filtering is essential to minimize phase noise and retrieve surface information that is present in the phase of the interferogram. In this study, adaptive Goldstein filter was applied to identify subsidence fringes (Goldstein and Werner 1998). The topography phase of the interferogram

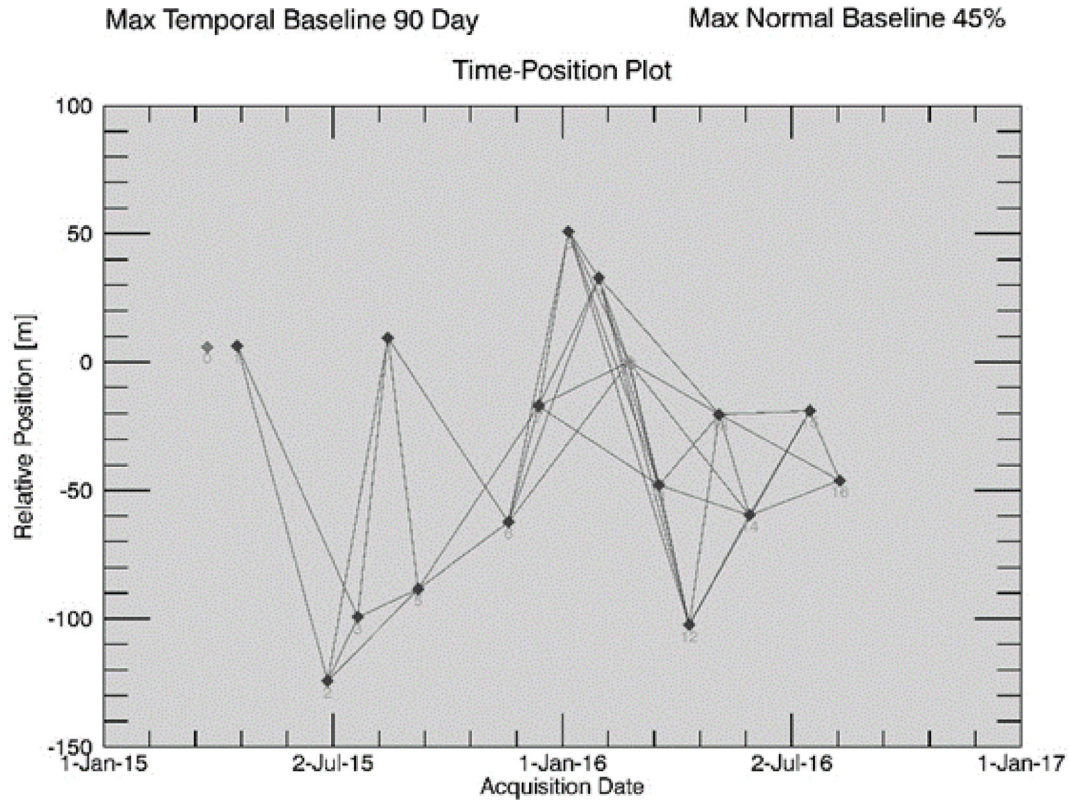


Figure 7. Graph of normal and temporal baselines of the Sentinel-1 data used in this study compared to the first image.

Table 1. Normal and temporal baselines and average coherency on the study area for selecting interferograms

Time period	Master date	Slave date	Normal baseline (m)	Absolute time baseline (day)	Coherency average on the study of area
t_1	3/24/2015	8/15/2015	12.79	144	0.449
t_2	8/15/2015	12/13/2015	- 28.96	120	0.442
t_3	12/13/2015	5/5/2016	- 5.86	144	0.443
t_4	5/5/2016	8/9/2016	- 26.82	96	0.552
t_5	3/24/2015	8/9/2016	- 48.473	504	0.351

was measured using only modulo- 2π (i.e., values range from 0 to 2π and then repeat) (Sarmap 2009). Phase unwrapping is the process for resolving this 2π ambiguity. Differential interferograms after filtering and unwrapping for t_1 to t_5 time periods are depicted in Figure 8.

RESULTS AND DISCUSSION

We analyzed four interferograms to monitor land subsidence in the study area covering a period of 14 months. Figure 9 presents the spatial distribution of land subsidence obtained from Sentinel-1

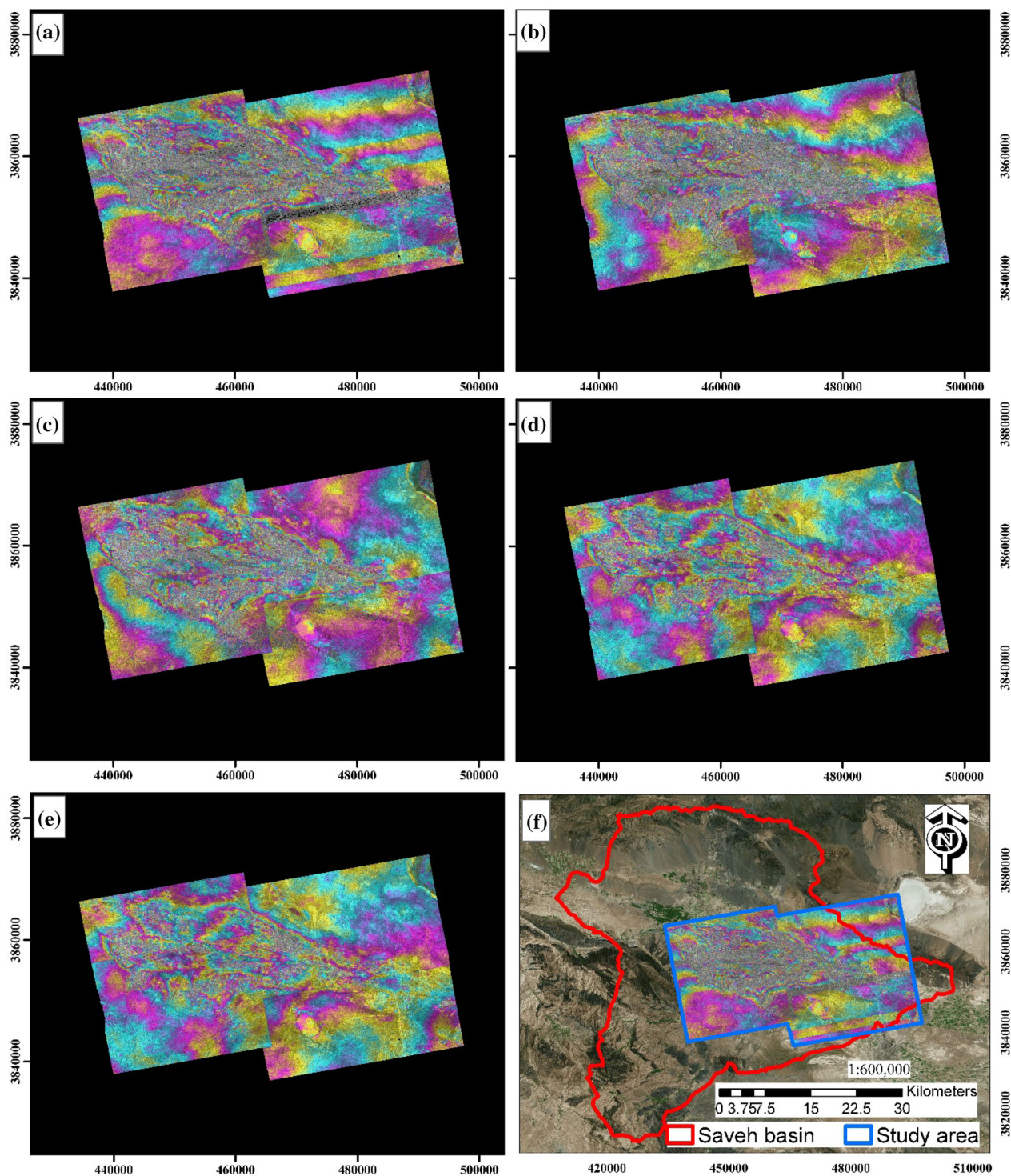


Figure 8. Differential interferograms after filtering and unwrapping during time periods (a) t_1 , (b) t_2 , (c) t_3 , (d) t_4 , and (e) t_5 . The location of the selected region for differential interferograms relative to the Saveh study area (f).

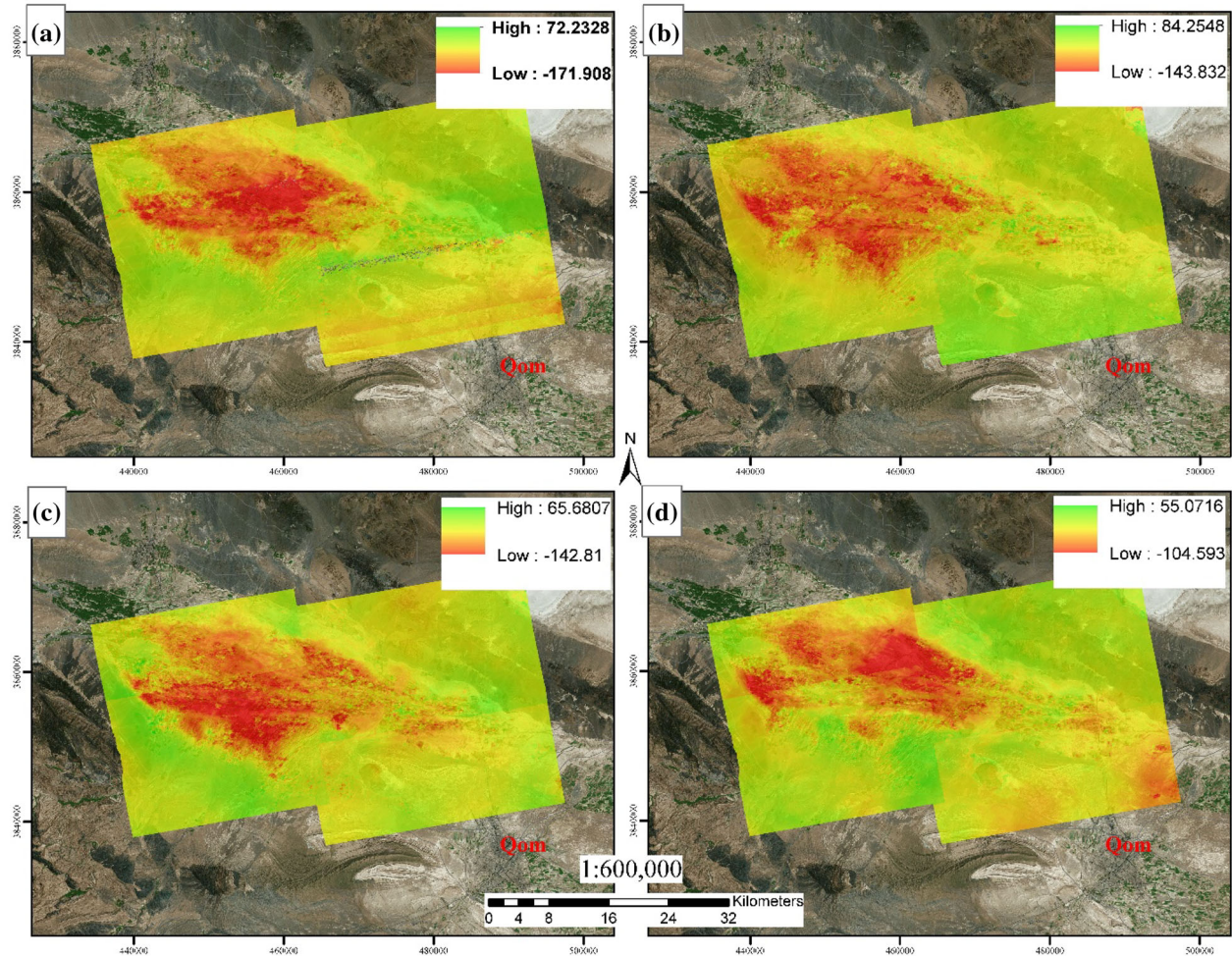


Figure 9. Displacement map (mm) obtained from unwrapped interferograms, during time periods **a** t_1 , **b** t_2 , **c** t_3 , and **d** t_4 .

InSAR analysis for four pairs of interferograms in the study area. As shown in this Figure, the subsidence level is higher on the west side than in the east side. The maximum subsidence is 171 mm for t_1 , 143 mm for t_2 , 142 mm for t_3 , and 104 mm for t_4 . Time difference between slave and master images, and probably variation in subsidence level with changes in the four time periods. The image also shows that subsidence in the study area is a continuous phenomenon and has relatively uniform spatial distribution.

Vertical displacement velocity map for the entire study period (t_5) and groundwater change contours from 2002 to 2015 is illustrated in Figure 10. It is noteworthy that the groundwater level for all piezometers data is available since 2002 (Abkhan consulting engineers 2013). As shown in Figure 10, the maximum groundwater decline during 2002 to 2015 period was 44 m, while the maximum subsidence rate of the study area during the total study period (t_5) was about 178 mm/year. The spatial distribution of subsidence shows that land deformation values decrease from west to east. Similarly,

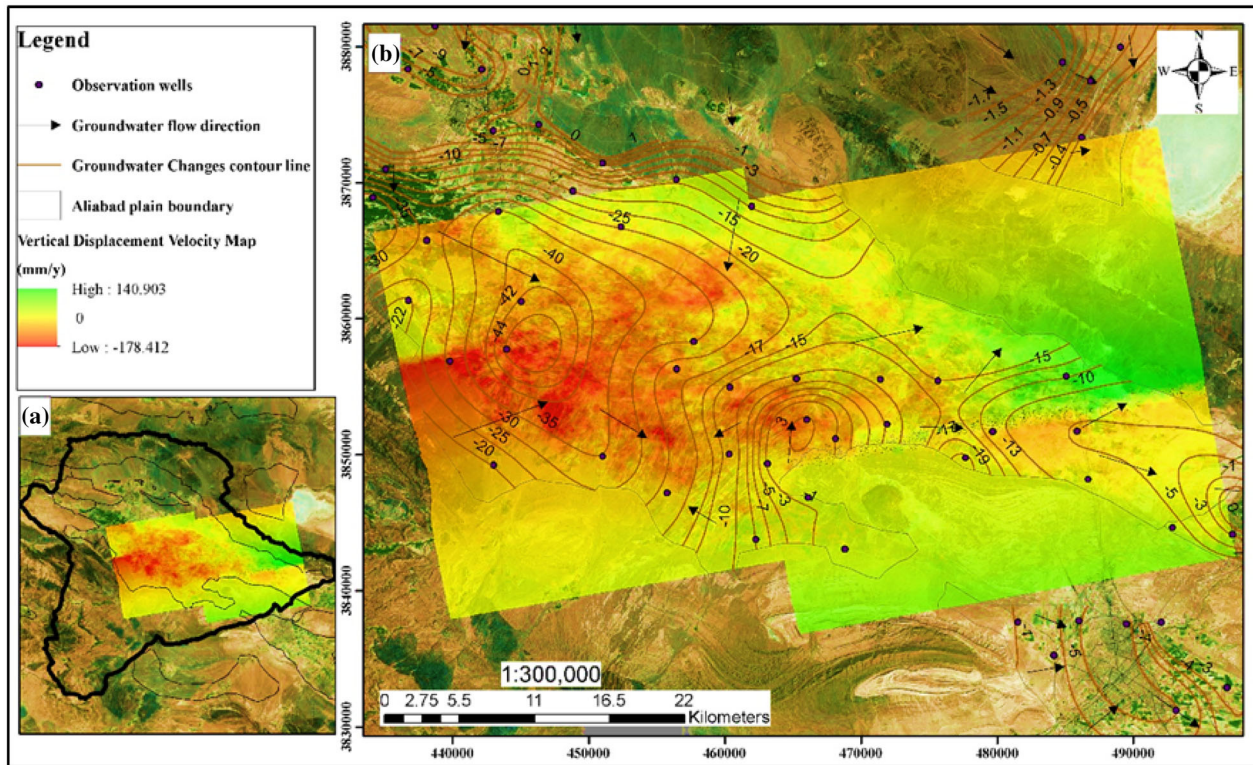


Figure 10. (a) Location of the study area relative to the Saveh study area. (b) Map of vertical displacement velocity (mm/year) in Aliabad plain during period t_5 .

groundwater reduction in the study area was higher in the west side than in the east side. In order to illustrate the relation between these two parameters, the graph of land deformation changes versus groundwater decline along profile A–B is shown in Figure 11. The longitudinal direction of profile A–B is from west to east and covers the whole study area. Curves fitted to these two graphs (red curves in Fig. 11b and c) have similar trends. Also, the maximum subsidence along profile A–B occurred where there the groundwater decline was maximum. Moreover, as can be seen from these Figures, the maximum cumulated subsidence in the study area was about 246 mm.

The graph of land deformation variations versus thickness of alluvium on profile A–B (Fig. 12) shows that the thickness of alluvium varies from 20 m at the margin of the plain to 280 m at the center of the

study area. Moreover, the results show that although curves fitted to the graphs (red curves in Fig. 12b and c) are ascending, the trends of these graphs are not entirely similar in profile A–B. Furthermore, areas with high thickness of alluvium in the study area have not necessarily experienced larger subsidence. This result suggests the lack of any direct meaningful relationship between these two parameters in the study area.

In Figure 13, the transmissivity contour line is shown. Based on this map, the values of transmissivity vary from $100 \text{ m}^2/\text{day}$ at the margin of the study area to $3000 \text{ m}^2/\text{day}$ at the Qarah-Chay Riverbank. In the center of the eastern part of the study area and around the Qarah-Chay River, the transmissivity values are $1500 \text{ m}^2/\text{day}$. To the margin of the study area, due to the decrease in thickness of alluvial deposits, the values are reduced to

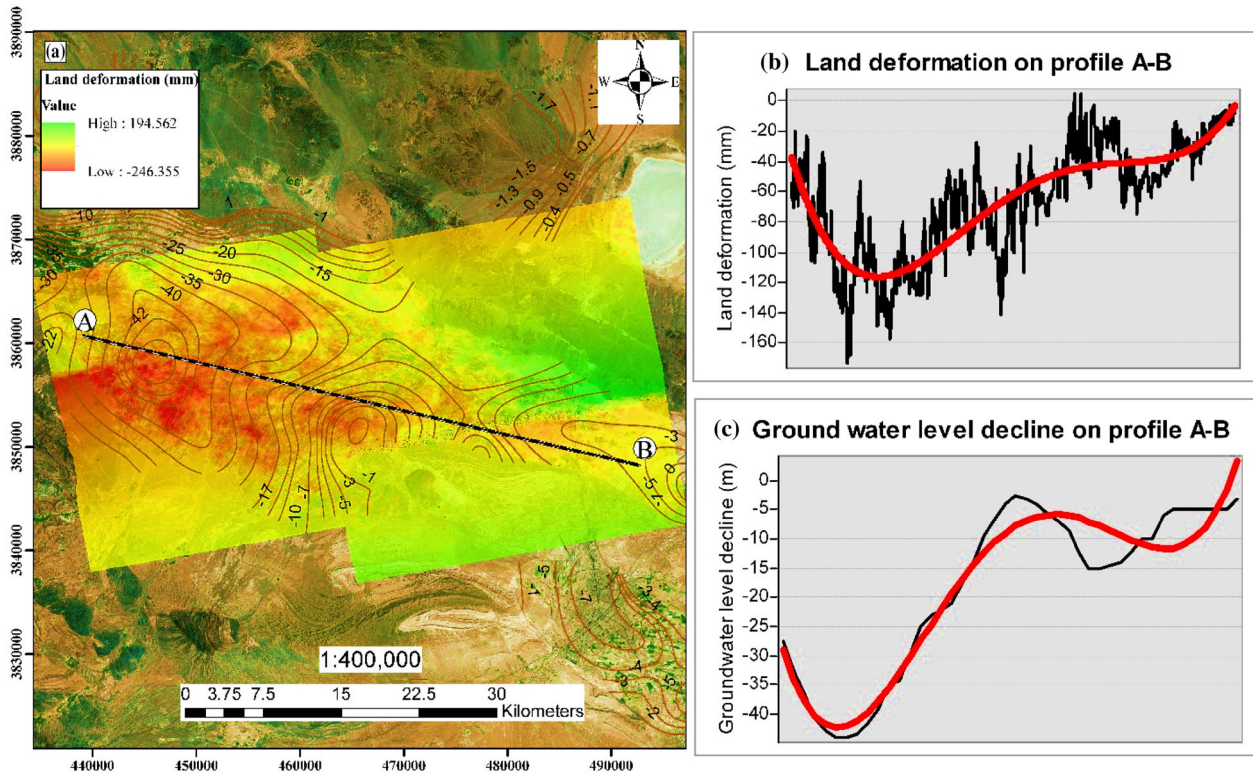


Figure 11. (a) Map of displacement (mm) obtained from unwrapped interferogram during period t_5 , showing groundwater contour line and position of profile A–B. (b) Land deformation along profile A–B. (c) Groundwater level decline along profile A–B. Red curves show fit curve of the graphs.

100 m²/day. Because of decreasing transmissivity, the subsidence level also decreased to the margin of the study area. Because alluvial deposits on the northern coast of Qarah-Chay River are coarse-grained, the distances between transmissivity contours in the northern coast are greater than in the south coast of the river. In the west of the study area, due to the presence of coarse-grained alluvial deposits and sediments from the Mazlaghan and Qarah-Chay rivers, transmissivity values are 1000 and 2000 m²/day, respectively, in most of this region. As shown in Figure 13b, curves fitted to transmissivity changes are descending from the west to east along profile A–B. The subsidence level also decreases from west to east of the study area (red curve in Fig. 13b). According to Figures 12c and 13c, transmissivity is reduced from the first one-third of the

plain toward the east due to a decrease in sediments thickness. This result can be seen also from the relation $T = Kb$, where b , K , and T , respectively, denote aquifer thickness, hydraulic conductivity, and transmissivity. In addition, moving toward the western parts of the plain and near the Qarah-Chay River, depending on geological diversity and thickness of the aquifer, hydraulic conductivity affects variations (increase) in transmissivity. The trend of variations in these diagrams markedly confirms ground deformation (Fig. 13b) from west to east in the plain.

Figure 14 presents the water level models and 3D diagrams for a part of the study area where log information of the wells is available. These 3D diagrams illustrate lithological information from 10 observation wells, amount of land deformation,

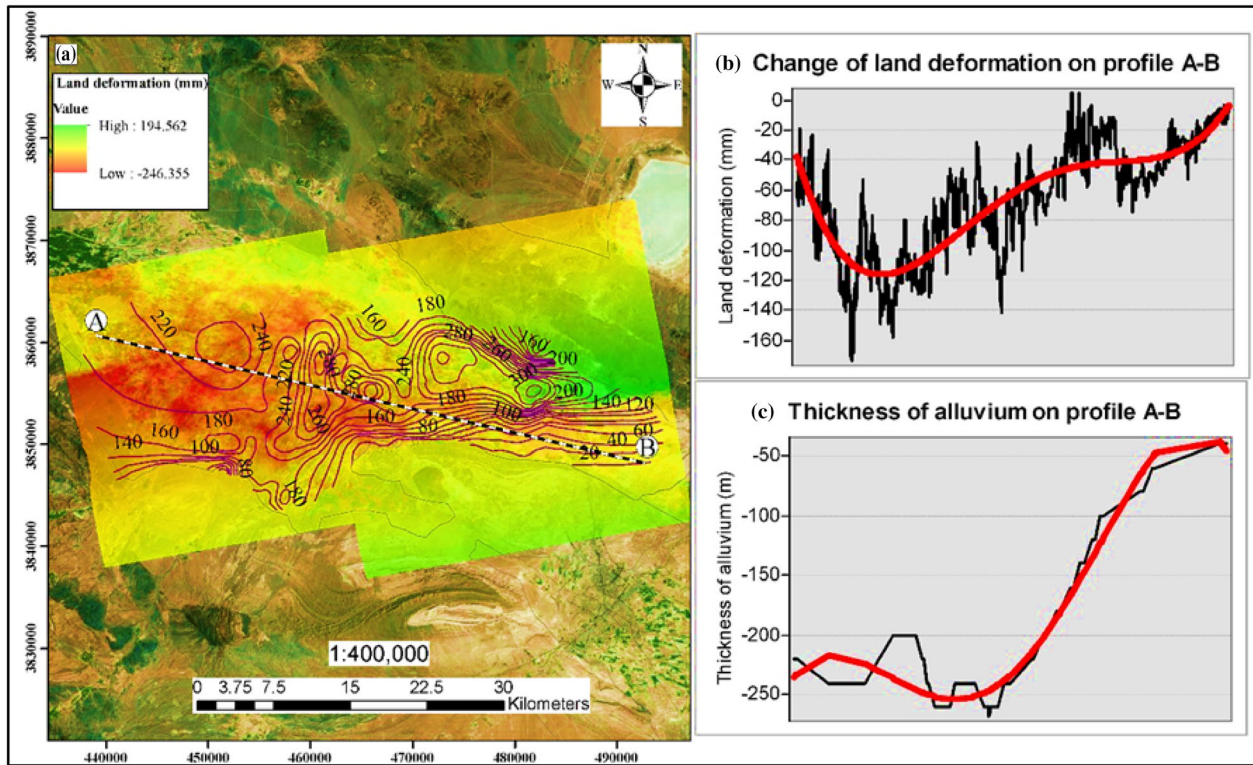


Figure 12. (a) Map of displacement (mm) obtained from unwrapped interferogram during period t_5 , showing thickness of alluvium contour line and position of profile A–B. (b) Land deformation along profile A–B. (c) Thickness of alluvium along profile A–B. Red curves show fit curve of the graphs.

groundwater level at the start and the end of the study period, and groundwater decline in the selected region.

According to Figure 14, due to the presence of coarse-grained sediments such as gravel and sand in the western part of the selected region, the groundwater level at the start of the study period in the western part (piezometers 1 and 2) is lower than in the eastern part (piezometers 4 to 10). Moreover, the decline rate in groundwater level during the study period in the western part is greater than that in the eastern part. As a result, the water level in piezometers 1 and 2 is lower compared with the other piezometers, indicating much greater subsidence level in the western part than in the eastern part of the plain.

CONCLUSIONS

In this research, the InSAR technique was applied to study land subsidence in the Aliabad plain, in central Iran. For this purpose, Sentinel-1 SLC images were acquired and DInSAR method was applied. Some images were selected from 24/03/2015 and 8/09/2016 to examine the spatial distribution and trends of subsidence in different seasons. The results showed that subsidence in this area is a continuous phenomenon and has relatively uniform spatial distribution. In a 14-month study, the maximum subsidence rate was 170 mm/year while the maximum accumulated subsidence was about 240 mm. Furthermore, we investigated the relationship between land deformation and parameters including

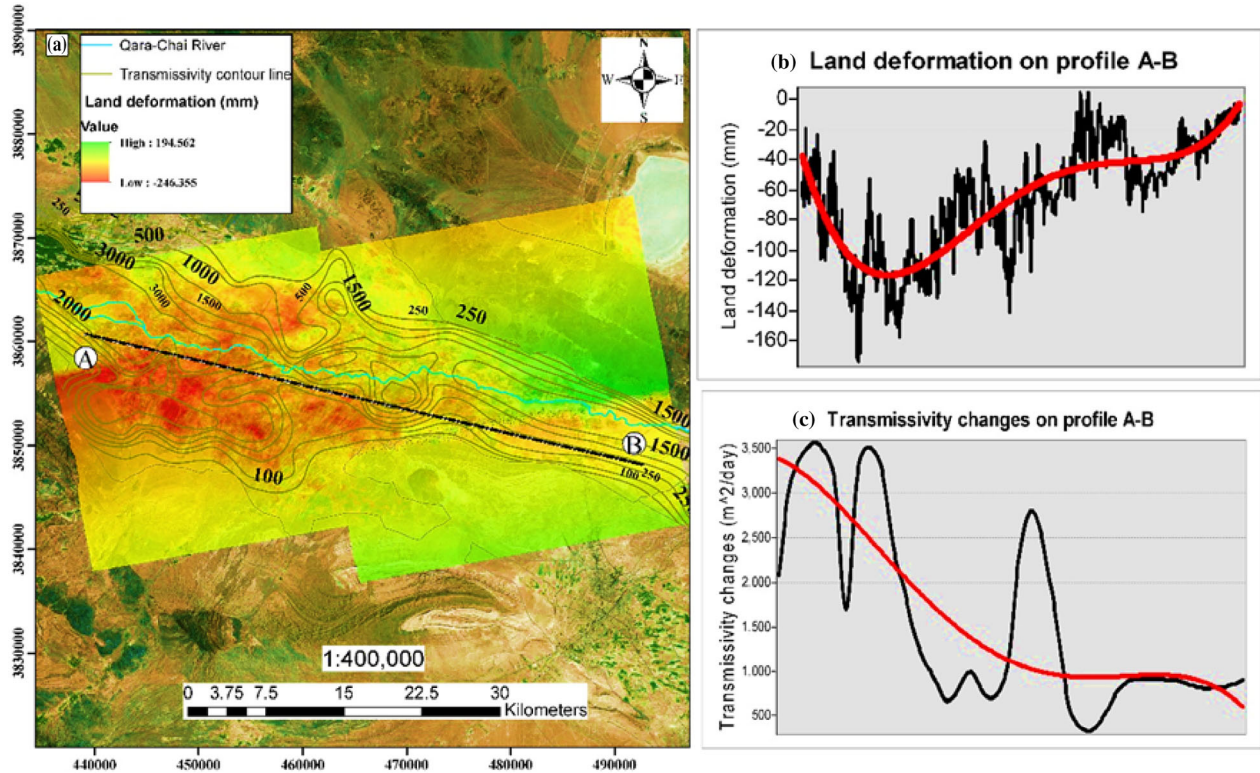


Figure 13. (a) Map of displacement (mm) obtained from unwrapped interferogram during t_5 period, showing transmissivity contour line and position of profile A–B. (b) Land deformation along profile A–B. (c) Transmissivity changes along profile A–B. Red curves show fit curve of the graphs.

groundwater changes, thickness of alluvium, and amount of transmissivity in the study area. The results showed a direct relation between the spatial distributions of land deformation level and groundwater decline. Moreover, studying land deformation in comparison with thickness of alluvium in the study area revealed that there is no meaningful relationship between these two parameters. The results showed that similar to decrease in transmissivity

values, subsidence level also declined from west to east in the study area.

Moreover, the 3D diagrams obtained from well logs showed that grain size distribution is one of the factors that affect subsidence level in the study area. The limitations of this study include lack of comprehensive databases and previous studies on this subject in the study area. In addition, few observation wells, shortage of comprehensive geotechnical

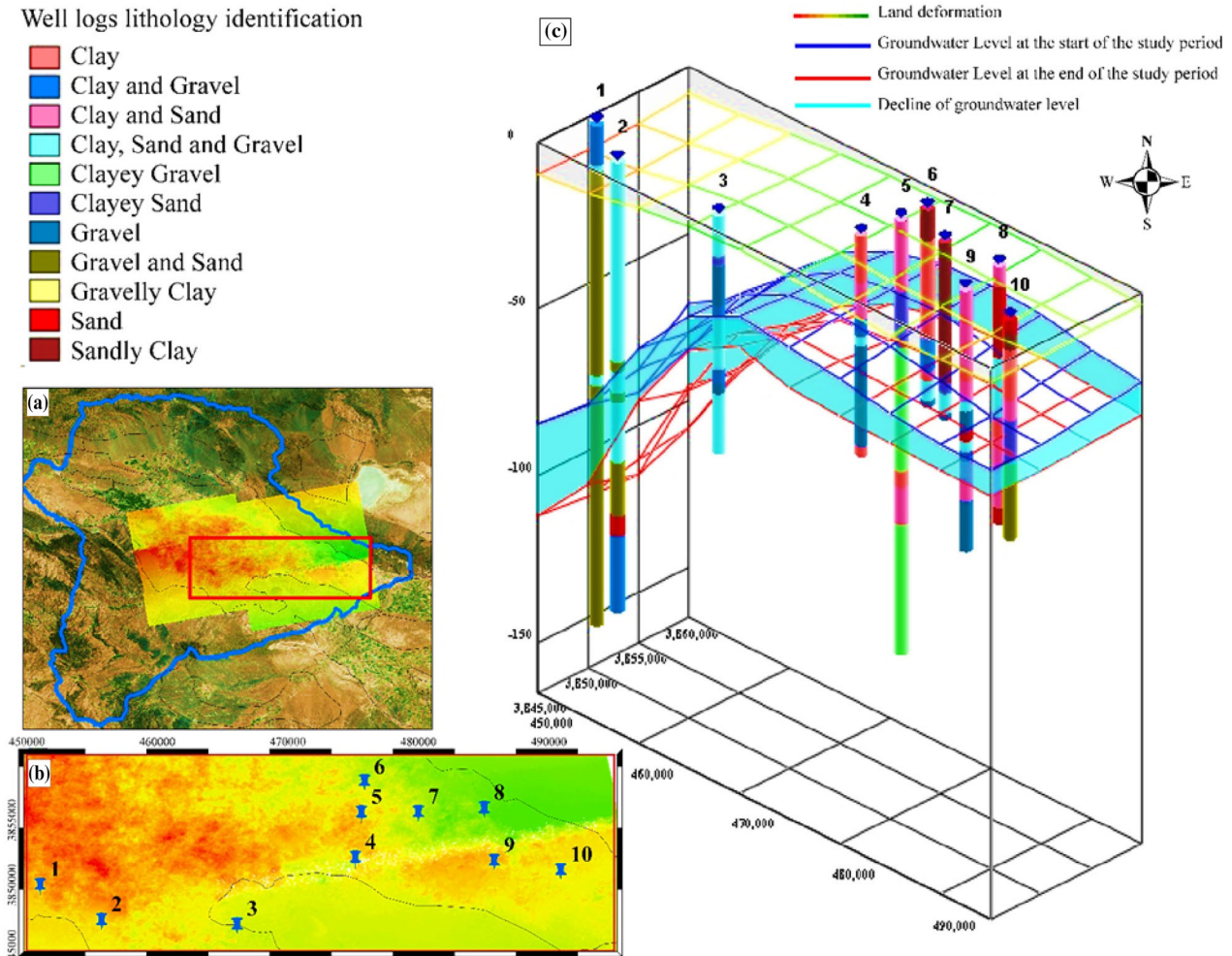


Figure 14. (a) Location of the selected region for 3D diagrams relative to the Saveh study area. (b) Position of piezometers in the selected region. (c) Water level models and 3D diagrams for selected area.

information, and lack of GPS stations for monitoring subsidence make the validation of the results of the study difficult.

ACKNOWLEDGMENTS

The Sentinel-1 IW SLC data used in this paper were provided by the European Space Agency through the Sentinel-1 Scientific Data Hub (Sentinel-1 Scientific Data Hub 2016). Finally, the authors wish to thank Prof. Sharifikia, Department of the Remote Sensing University of Tarbiat Modares for providing ENVI SAR scape 5.2 dongle license.

REFERENCES

Ahmad, W., Choi, M., Kim, S., & Kim, D. (2017). Detection of land subsidence due to excessive groundwater use varying with different land cover types in Quetta valley, Pakistan using ESA-sentinel satellite data. *Natural Hazards and Earth System Sciences*. <https://doi.org/10.5194/nhess-2017-234>.

Bates, R. L., & Jackson, J. A. (1987). *Glossary of geology*. Alexandria: American Geological Institute.

Boni, R., Herrera, G., Meisina, C., Notti, D., Béjar-Pizarro, M., Zucca, F., et al. (2015). Twenty-year advanced DInSAR analysis of severe land subsidence: The Alto Guadalenín Basin (Spain) case study. *Engineering Geology*, 198, 40–52.

Davoodijam, M., Motagh, M., & Momeni, M. (2015). Land subsidence in Mahyar Plain, Central Iran, investigated using Envisat SAR data. In *The 1st international workshop on the quality of geodetic observation and monitoring systems (QU-GOMS'11)* (pp. 127–130). Springer, Cham.

- De Zan, F., & Guarnieri, A. M. M. (2006). TOPSAR: Terrain observation by progressive scans. *IEEE Transactions on Geoscience and Remote Sensing*, 44(9), 2352–2360.
- Fiaschi, S., Tessitore, S., & Bon, R. (2017). From ERS-1/2 to sentinel-1: Two decades of subsidence monitored through A-DInSAR techniques in the Ravenna area (Italy). *GIScience and Remote Sensing*, 54(3), 305–328.
- Galloway, D. L., & Burbey, T. J. (2011). Review: Regional land subsidence accompanying groundwater extraction. *Hydrogeology Journal*, 19(8), 1459–1486.
- Gambolati, G., Teatini, P., & Ferronato, M. (2006). Anthropogenic land subsidence. In *Groundwater* (Vol. 13, pp. 2443–2459). Encyclopedia of Hydrological Sciences.
- Goldstein, R. M., & Werner, C. L. (1998). Radar interferogram filtering for geophysical applications. *Geophysical Research Letters*, 25(21), 4035–4038.
- Holzer, T. L., & Galloway, D. L. (2005). Impacts of land subsidence caused by withdrawal of underground fluids in the United States. *Reviews in Engineering Geology*, 16, 87–99.
- Lashkaripour, G., Ghafouri, M., & Salehi, R. (2010). Land subsidence of southern Mahyar plain and effects of induced fissures on residential, industrial and agricultural. In *Paper presented at the fifth national conference of geology and the environment*. Iran: Islamic Azad University of Eslamshahr. (In Persian).
- Mahmoudpour, M., Khamehchiyan, M., Nikudel, M. R., & Ghassemi, M. R. (2016). Numerical simulation and prediction of regional land subsidence caused by groundwater exploitation in the southwest plain of Tehran, Iran. *Engineering Geology*, 201, 6–28.
- Rajabi, A. M. (2018). A numerical study on land subsidence due to extensive overexploitation of groundwater in Aliabad plain, Qom-Iran. *Natural Hazards*, 93(2), 1085–1103.
- Rajabi, A. M., & Ghorbani, E. (2016). Land subsidence due to groundwater withdrawal in Arak plain, Markazi Province, Iran. *Arabian Journal of Geosciences*, 9(20), 738.
- Rezaei Kalantari, R., Yari, A. R., Ahmadi, E., Azari, A., Tahmasbi Zade, M., & Gharagazlo, F. (2013). Survey of corrosion and scaling potential in drinking water resources of the villages in Qom province by use of four stability indexes (with quantitative and qualitative analysis). *Archives of Hygiene Sciences*, 2(4), 127–134.
- Sarmap SA. (2009). *Synthetic Aperture Radar and SARscape: SAR Guidebook* (p. 274). Purasca, Switzerland: Sarmap SA.
- Sarmap SA. (2015). ENVI SARscape 5.2. (5.2.1.201700109W64 ed.). Switzerland: 2015 sarmap SA.
- Sentinel-1. (2016). <https://sentinels.copernicus.eu/web/sentinel/mis-sions/sentinel-1>. Accessed 12 May 2017.
- Sentinel-1 Scientific Data Hub. (2016). <https://scihub.copernicus.eu/>. Accessed 12 Mar 2017.
- Sharifikia, M. (2010). Evaluation of land subsidence related disasters in plains and residential areas of Iran. *Iranian Association of Engineering Geology*, 3(3), 43–58.
- Siles, G. L., Alcérreca-Huerta, J. C., López-Quiroz, P., & Hernández, J. C. (2015). On the potential of time series InSAR for subsidence and ground rupture evaluation: Application to Texcoco and Cuautitlan-Pachuca subbasins, northern Valley of Mexico. *Natural Hazards*, 79(2), 1091–1110.
- Toms, R., Romero, R., Mulas, J., & Marturi, J. J. (2014). Radar interferometry techniques for the study of ground subsidence phenomena: A review of practical issues through cases in Spain. *Environmental Earth Sciences*, 71(1), 163–181.
- Water Resources Report of Saveh Study Area. (2013). *Iran water resources management*. Water Utility Company in Qom: Abkhan Consulting Engineers (in Persian).
- Wegmüller, U., Werner, C., Wiesmann, A., Strozzi, T., Kourkoui, P., & Frey, O. (2016). Time-series analysis of Sentinel-1 interferometric wide swath data: Techniques and challenges. *2016 IEEE International Geoscience and Remote Sensing Symposium (IGARSS)*, pp. 3898–3901.
- Yan, Y., Doin, M.-P., Lopez-Quiroz, P., Tupin, F., Fruneau, B., Pinel, V., et al. (2012). Mexico city subsidence measured by InSAR time series: Joint analysis using PS and SBAS approaches. *IEEE Journal of Selected Topics in Applied Earth Observations and Remote Sensing*, 5(4), 1312–1326.
- Zhu, L., Gong, H., Li, X., Wang, R., Chen, B., Dai, Z., et al. (2015). Land subsidence due to groundwater withdrawal in the northern Beijing plain, China. *Engineering Geology*, 193, 243–255.